Molecular Biology of the Cell
Vol. 9, 2873–2889, October 1998

A Yeast t-SNARE Involved in Endocytosis

Karin Séron,* Ville Tieaho,† Cristina Prescianotto-Baschong,‡ Thomas Aust,‡ Marie-Odile Blondel,* Philippe Guillaud,* Ginette Devilliers,* Olivia W. Rossanese,§ Benjamin S. Glick,§ Howard Riezman,‡ Sirkka Keränen,† and Rosine Haguenauer-Tsapis*‖

*Institut Jacques Monod, Centre National de la Recherche Scientifique-UMRC7592, Université Paris 7-Denis Diderot, Paris Cedex 05, France; †VTT Biotechnology and Food Research, FIN-02044 VTT, Finland; ‡Biozentrum, University of Basel, CH-4056 Basel, Switzerland; and §Department of Molecular Genetics and Cell Biology, The University of Chicago, Chicago, Illinois 60637

Submitted April 6, 1998; Accepted July 31, 1998
Monitoring Editor: Randy W. Schekman

The ORF YOL018c (*TLG2*) of *Saccharomyces cerevisiae* encodes a protein that belongs to the syntaxin protein family. The proteins of this family, t-SNAREs, are present on target organelles and are thought to participate in the specific interaction between vesicles and acceptor membranes in intracellular membrane trafficking. *TLG2* is not an essential gene, and its deletion does not cause defects in the secretory pathway. However, its deletion in cells lacking the vacuolar ATPase subunit Vma2p leads to loss of viability, suggesting that Tlg2p is involved in endocytosis. In *tlg2*Δ cells, internalization was normal for two endocytic markers, the pheromone α-factor and the plasma membrane uracil permease. In contrast, degradation of α-factor and uracil permease was delayed in *tlg2*Δ cells. Internalization of positively charged Nanogold shows that the endocytic pathway is perturbed in the mutant, which accumulates Nanogold in primary endocytic vesicles and shows a greatly reduced complement of early endosomes. These results strongly suggest that Tlg2p is a t-SNARE involved in early endosome biogenesis.

INTRODUCTION

The transport of proteins along the secretory and endocytic pathways occurs in membrane-enclosed vesicles that bud from the donor membrane and fuse with the proper target membrane. The SNARE hypothesis (Söllner *et al*., 1993) predicts that the specificity of the targeting event is at least partially determined by interactions between membrane proteins residing in the vesicle, v-SNAREs, and in the target membrane, t-SNAREs. These proteins were originally identified as receptors of the soluble *N*-ethylmaleimide-sensitive fusion (NSF) attachment protein SNAP, which together with the NSF protein (Sec18p in *Saccharomyces cerevisiae*), are involved in the process that finally leads to fusion of the vesicle and the target membrane. The soluble NSF and SNAP proteins function in multiple targeting steps, either in priming SNARE complex formation or in breaking down the complex linked to the fusion process itself (Hay and Scheller, 1997; Götte and Fischer von Mollard, 1998). In addition to these general vesicle fusion factors, several specific soluble components are involved in the targeting and fusion of transport vesicles, for instance, the members of the Sec1 protein family (Aalto *et al*., 1992) and the small GTPases of the Rab family (Novick and Zerial, 1997). Although both protein families have been implicated as regulators of SNARE complex formation, the exact molecular events leading to fusion remain elusive.

Several v- and t-SNAREs functioning at different steps along the secretory pathway have been described for yeast and for mammalian cells (Hay and Scheller, 1997; Götte and Fischer von Mollard, 1998). The prototypes of the t-SNAREs are syntaxins, which in mammalian neurons target the synaptic vesicles at the presynaptic active zone (Bennett *et al*., 1992). In *S. cerevisiae*, the syntaxin homologues are the Sso1 and Sso2 proteins that are involved in Golgi to plasma membrane trafficking (Aalto *et al*., 1993). Other t-SNAREs that are homologous to the Sso proteins

‖ Corresponding author. E-mail address: haguenauer@ijm.jussieu.fr.

Table 1. Strains used in this study

Strains	Genotype	Source
FY1679	*MAT***a**/α *ura3-52/ura3-52 leu2Δ1/+ trp1Δ63/+ his3Δ200/+*	Winston *et al*., 1995
FHER001	*MAT***a**/α *tlg2*::*KanMX4 ura3-52/ura3-52 leu2Δ1/+ trp1Δ63/+ his3Δ200/+*	This study
FHER001-05A	*MAT*α *tlg2*::*KanMX4 ura3-52 leu2Δ1*	This study
FHER001-03B	*MAT*α *ura3-52 leu2Δ1 his3Δ200*	This study
WHER-BMA64	*MAT*α, *ura3-1, trp1-Δ2, leu2-3,112, his3-11, ade2-1; can1-100*	P. Slonimski
WHER006-03B	*MAT*α, *tlg2*::*KanMX4 ura3-1, trp1-Δ2, leu2-3,112, his3-11, ade2-1; can1-100*	This study
NY3	*MAT***a** *sec1-1 ura3-52*	P. Novick
NY24	*MAT***a** *sec1-11 ura3-52*	P. Novick
YW21-1A	*MAT*α *slp1*::*LEU2 leu2 ura3 trp1 his3 ade2 lys2*	Y. Wada/Y. Anraku
RPY12	*MAT*α *vps45Δ pep4*	T. Stevens
RPY15	*MAT*α *vps45-ts3 pep4-3 leu2-3 ura3-52 his4-519 ade6 gal2*	T. Stevens
312xxa	*MAT***a** *sly1-ts leu2-3,112 ura3-1 trp1 ade2-1*	J. R. Warner
RH3419	*MAT***a** *ura3 leu2 vma2*::*LEU2 his3 ade2 ade3 lys2 bar1-1*/pHR7	H. Riezman lab
RH475-8C	*MAT***a** *ura3 leu2 his3 ade2 ade3 lys2 bar1-1*	H. Riezman lab
RH4074	RH475-8C *tlg2*::*KanMX4*	This study
RH4075	RH3419 *tlg2*::*KanMX4*	This study
SL	*MAT*α *sec18-1 leu2-3, 2-112*	Volland *et al*., 1994

function at different steps along the secretory pathway, such as Sed5p between endoplasmic reticulum (ER) and Golgi, and Ufe1p between Golgi and ER (retrograde transport) (Pelham, 1998). Although many trafficking events appear to involve vesicle budding and fusion, the mechanism of transport through the endosomal system remains more controversial. It is not yet clearly established whether endocytic compartments are part of a dynamic continuum or are stable structures in communication by vesicular transport. It is therefore critical to know whether t-SNAREs are involved at the successive steps of the endocytic pathway.

S. cerevisiae internalizes small molecules by both fluid phase and receptor-mediated endocytosis. Endocytosis also plays a key role in the turnover of plasma membrane proteins. On their way from the plasma membrane to the vacuole, internalized molecules and proteins move through two biochemically separable membrane-bound compartments, defined as the yeast early and late endosomes (Singer-Krüger *et al*., 1993). The latter may correspond to the prevacuolar compartment, involved in the traffic of vacuolar proteins from the late Golgi to the vacuole (Jones *et al*., 1997). Transit from Golgi to the prevacuolar compartment has been extensively studied and was shown to require among others Sec18p, the Sec1p homologue Vps45p, and the t-SNARE Pep12p (Becherer *et al*., 1996; Burd *et al*., 1997), which might be located on the prevacuolar organelle (Becherer *et al*., 1996). The t-SNARE Vam3p, associated with the vacuolar membrane (Wada *et al*., 1997), may function together with the Sec1p homologue Vps33/Slp1p and the Rab protein Ypt7p in late endosome to vacuole transport (Jones *et al*., 1997), as well as in vacuolar fusion (Haas *et al*., 1995; Nichols *et al*., 1997; Wada *et al*., 1997). Numerous genes involved in the internalization step of endocytosis have been identified (Geli and Riezman, 1998). However, transit from early to late endosomes remains far less understood. Yeast early endosomes are still poorly defined. The Rab5 homologue Ypt51p could reside both in this organelle and in late endosomes (Singer-Krüger *et al*., 1995), but the Ypt51p-dependent step in the endocytic pathway remains unclear (Horazdovsky *et al*., 1994). Recent investigations have led to visualization of early endosomes by immunofluorescence (Hicke *et al*., 1997) and by electron microscopy (Prescianotto-Baschong and Riezman, 1998). Here we report the identification of a t-SNARE of *S. cerevisiae* found by sequence comparisons with other t-SNARE proteins. We present evidence that this protein plays a role in the endocytic pathway. The function of this protein has also been examined recently by others (Abeliovich *et al*., 1998; Holthuis *et al*., 1998).

MATERIALS AND METHODS

Sequence Analysis

The hydrophobic cluster analysis (HCA) method (Callebaut *et al*., 1997) is based primarily on basic rules underlying the folding of globular proteins (hydrophilic surface vs. hydrophobic core). It uses a bidimensional plot in which the amino acid sequence of a protein is displayed as an unrolled and duplicated longitudinal cut of a cylinder, where the amino acid residues follow an α-helical pattern. The contours of the hydrophobic residues (Val, Ile, Leu, Met, Phe, Trp, and Tyr) are automatically drawn. The α-helical net has been shown to offer the best correspondence between the positions of hydrophobic clusters and regular secondary structures. Some amino acids known to have specific structural behavior are represented by symbols: ⊡ for serine, □ for threonine, ◆ for glycine, and ★ for proline. HCA plots were performed using the DrawHCA program available at http://www.lmcp.jussieu.fr/~mornon.

Strains, Plasmids, and Growth Conditions

The strains used in this study are listed in Table 1. Standard genetic techniques were used. Cells were transformed according to Gietz *et*

al. (1992). Because the chromosome-encoded uracil permease is produced in very low amounts, cells expressing the permease from a multicopy plasmid were used to immunodetect the protein. The multicopy plasmids p195gF (2μ *URA3 GAL-FUR4*) and pgF (2μ *LEU2 GAL-FUR4*) carry the *FUR4* gene under the control of the *GAL10* promoter (Volland *et al*., 1994).

Cells were grown at 30°C (24°C for temperature-sensitive mutants) in rich YPD medium (1% yeast extract, 2% peptone, and 2% glucose) or in defined YNB minimal medium containing 0.67% yeast nitrogen base without amino acids (Difco, Detroit, MI) supplemented with appropriate nutrients (Sherman *et al*., 1983). The carbon source was 2% glucose, 4% galactose plus 0.02% glucose, or 2% lactate.

Inactivation of the TLG2 Locus

An ORF replacement cassette with long flanking homology regions was used to disrupt the *TLG2* gene (Wach, 1996). PCR amplification using *Pwo* DNA polymerase (Boehringer Mannheim, Indianapolis, IN) from the genomic DNA of the FY1679 strain with four oligonucleotide primers, L1 (5′-GTACGTACCTGGTAATGAGCAGGCCG-3′), L2 (5′-GGGGATCCGTCGACCTGCAGCGTACCATGTTTG-TAACGACTGCCTAG-3′), L3 (5′-AACGAGCTCGAATTCATC-GATGATATGATGACAAAACTTTCACGG-3′), and L4 (5′-CTA-CGTACACAATAACCACCAACTTG-3′), generated two DNA products corresponding to the *TLG2* promoter and terminator, respectively, with 25-bp extensions (underlined) homologous to the *KanMX4* marker (Wach *et al*., 1994) containing the geneticin (G418) resistance gene. In a second PCR amplification experiment, one strand of each of these molecules served as a long primer using *KanMX4* as template. The linear fragment was used to transform FY1679, leading to strain FHER001 resistant to G418. Correct integration at the *TLG2* locus was confirmed by whole-cell PCR using *TLG2*- and *KanMX4*-specific primers. Haploid strains were obtained from the diploid strain after tetrad dissection. Two haploid strains (one undisrupted, FHER001-3B, and one disrupted, FHER001-5A) were used in further experiments. The disruption cassette was cloned in *Eco*RV-cut pUG7 (Güldener, Heck, and Hegemann, unpublished data). The cassette was released by *Not*I and used to disrupt *TLG2* in other genetic backgrounds, such as W303-BMA64, leading to WHER006-3B.

Cloning of the Chromosomal Gene

The disruption cassette described above was cloned into the *Sma*I site of a modified pFL38 (CEN/ARS *URA3*) (Bonneaud *et al*., 1991) in which a sequence in the multiple cloning site extending from *Eco*RI to *Kpn*I was removed. Promoter and terminator regions were verified by sequencing. The *KanMX4* module was removed by *Sma*I–*Ecl*II digestion. The resulting linear plasmid was purified from an agarose gel with Jetsorb (Genomed GmbH, Bad Oeynhausen, Germany) and used to transform the wild-type FHER001-3B strain for gap repair. Transformants were selected on YNB medium without uracil. Plasmids were extracted from pooled yeast colonies and used to transform DH5-α-competent cells (Life Technologies, Gaithersburg, MD). Clones were checked with the appropriate restriction enzymes, and pYCG-YOL018c was sequenced in the region corresponding to the C-terminal part of the protein.

Construction of HA- and GFP-tagged Tlg2p

To construct the HA-tagged version of the Tlg2p, the 5′ end of the gene (nucleotides 1–297) was amplified with oligonucleotide primers L5 (5′-GCATTGGATCCTCTAGATGTATCCGTATGATGTG-CCTGACTACGCAATGTTTAGAGATAGAACT-3′), containing *Bam*HI and *Xba*I sites and the coding sequence for nine amino acids of hemagglutinin (HA) (YPYDVPDYA), and L6 (5′-GCCAGGTA-ACGAATTCTTCC-3′), containing an *Eco*RI site. The resulting fragment was ligated into Bluescript II KS$^-$ (Stratagene, La Jolla, CA) as an *Xba*I–*Eco*RI fragment, and the clones were sequenced. Nucleotides 298-1194 of *TLG2* were obtained as an *Eco*RI–*Hin*dIII fragment from plasmid pYCG-YOL018c and subsequently joined with the PCR-generated fragment to complete the gene. The HA-*TLG2* was subcloned into the *Xba*I-digested pVT102U (2μ *URA3*) vector (Vernet *et al*., 1987), leading to pHA-TLG2, to obtain overexpression of the gene under the strong *ADH1* promoter.

For protein localization studies the *TLG2* gene was N-terminally tagged with the green fluorescent protein (GFP). Nucleotides 1–297 of the *TLG2* gene were amplified using oligonucleotide primers L7 (5′-GCATCTAGAATGTTTAGAGATAGAACT-3′) and L6 and subcloned as an *Xba*I–*Eco*RI fragment into Bluescript II KS−. The sequenced PCR fragment was subsequently joined to the 3′ fragment of the gene. The entire gene was transferred into *Xba*I-digested pGFP-N-FUS (CEN6/ARSH4 *URA3*) (Niedenthal *et al*., 1996), leading to pGFP-TLG2, and the correct orientation of the insert was verified.

Construction of Sec7p-GFP

The endogenous chromosomal copy of *SEC7* was replaced with a *SEC7-GFP* fusion gene using the pop-in, pop-out method (Rothstein, 1991), as follows. The 3′ untranslated region of *SEC7* to the downstream *Sph*I site was amplified by PCR with the introduction of an *Sma*I site at the 5′ end of the fragment, and this sequence (1674 bp) was subcloned into pUC19 digested with *Sma*I and *Sph*I, generating pSEC7–3′. To create the integrating vector pUSE-URA3, the stop codon of *SEC7* was replaced with a *Bam*HI site, and this site was joined to the *Bam*HI site upstream of the *EGFP* gene in pEGFP-1 (Clontech, Palo Alto, CA) (sequence of the fusion junction: TAC CTT TCT ACG GAT CCA). An *Eco*RI to the blunted *Not*I fragment comprising the last 582 bp of *SEC7* fused to *EGFP* was subcloned into pSEC7–3′ digested with *Eco*RI and *Sma*I, generating pUSE. Then the *URA3* gene was excised from pUC1318-URA3 (Benedetti *et al*., 1994) as a *Hin*dIII fragment, blunted, and subcloned into the blunted *Aat*II site of pUSE, yielding pUSE-URA3. This construct was integrated into the *SEC7* locus by linearizing with *Spe*I and transforming strain FHER001-3B. Pop-in integrants were selected on minimal medium lacking uracil. The presence of Sec7p-GFP and the absence of wild-type Sec7p were confirmed by Western blotting of cell extracts using an anti-Sec7p antibody (a gift from A. Franzusoff, University of Colorado, Denver, CO).

Strains expressing Sec7p-GFP grow at the same rate as the parental strains (our unpublished results). To ensure that the GFP tag has no effect on Sec7p localization, cells expressing either wild-type Sec7p or Sec7p-GFP were transformed with pSN218 (Nothwehr *et al*., 1995); this plasmid encodes HA-tagged Kex2p. Kex2p is known to colocalize with Sec7p (Franzusoff *et al*., 1991). Double-label immunofluorescence using anti-Sec7p and anti-HA antibodies confirmed that Sec7p and Sec7p-GFP both exhibit punctate distributions that overlap strongly with the distribution of Kex2p-HA.

Measurement of Cell Surface Delivery of Uracil Permease

Uracil uptake, used to quantify the amount of the permease reaching the cell surface, was measured after permease induction in exponentially growing cells as previously described (Moreau *et al*., 1997). One milliliter of yeast culture was incubated with 5 μM [^{14}C]uracil (New England Nuclear, Boston, MA) for 1 min at 30°C and then quickly filtered through a Whatman (Maidstone, England) GF/C filter, which was washed twice with ice-cold water and counted for radioactivity.

Synthetic Lethality with vma2Δ

Experiments were performed according to the method of Munn and Riezman (1994), except that strain RH3419 containing plasmid pHR7 was used. Plasmid pHR7 was constructed by cloning a 2.7-kb

blunt-ended *Hin*dIII fragment carrying *VMA2* derived from pCY36 (provided by T. Stevens, University of Oregon, Eugene, OR) into the *Nru*1 site of pCH1122 (CEN4/ARS1 *URA3 ADE3*, provided by C. Holm, University of California, San Diego, CA).

Endocytosis Assays

α-Factor internalization assays were performed at 30°C after a 15-min preincubation by the continuous presence protocol (Dulic *et al*., 1991), and degradation assays were performed at 30°C after 50 min of binding of [^{35}S]α-factor at 0°C according to the method of Dulic *et al*. (1991).

Uracil uptake, used to quantify the amount of the cell surface permease, was measured as described above, except that incubation was performed for 20 s at either 37°C (see Figure 5A), or 30°C (see Figure 5C).

Yeast Cell Extracts and Western Immunoblotting

The proteins obtained from cell extracts were analyzed by immunoblots as previously described (Volland *et al*., 1994), using either an antiserum to the last 10 residues of uracil permease or an anti-carboxypeptidase Y (CPY) or an anti-alkaline phosphatase (ALP) antibody (Molecular Probes, Eugene, Oregon). Primary antibodies were detected with a horseradish peroxidase-conjugated anti-rabbit or anti-mouse immunoglobulin G secondary antibody followed by Boehringer Mannheim chemiluminescence kit. For the endoglycosidase H assay, protein extracts were diluted 13-fold in 0.1 M citrate buffer (pH 5.5) and incubated without or with 2 mU of endoglycosidase H (Boehringer Mannheim) for 3 h at 37°C. The proteins were then precipitated as described (Volland *et al*., 1994) and separated by conventional SDS-PAGE. The gel was blotted onto a nitrocellulose filter, and the HA-tagged Tlg2p was detected by using mouse monoclonal HA antibody (ascitic fluid containing the 12CA5 antibody). The primary antibody was detected with ALP-conjugated goat anti-mouse immunoglobulin G and revealed as described above.

Pulse–Chase Labeling and Immunoprecipitation of CPY

In pulse–chase experiments, yeast cells were grown in YNB medium with glucose as a carbon source to an A_{600} of 1 (2×10^7 cells/ml). They were collected and resuspended in fresh medium at an A_{600} of 5, labeled for 4 min by adding 150 μCi [^{35}S]methionine (Amersham, Arlington Heights, IL) per milliliter of culture and chased with 10 mM cold methionine. Aliquots of the culture (0.3 ml) were removed at various times during the chase, and cell extracts were prepared by lysis with 0.2 M NaOH for 10 min on ice. Trichloroacetic acid was added to a final concentration of 5%, and the samples were incubated for an additional 10 min on ice. The proteins were processed for immunoprecipitation as described previously (Moreau *et al*., 1996). The immunoprecipitated proteins were separated by SDS-PAGE on 7.5% gels and treated by fluorography.

Incubations with Positively Charged Nanogold and Analysis by Electron Microscopy

Spheroplasts were made according to the method of Kübler *et al*. (1994) with the following modifications. The cells were treated with 0.1 M Tris-HCl (pH 9.0) and 10 mM 2-mercaptoethanol for 10 min at room temperature and then washed once in 10 mM Tris-HCl (pH 7), 0.7 M sorbitol, 5% glucose and 0.5× YPUAD (YPD supplemented with 40 μg/ml each adenine and uracil), resuspended in the same solution at 1–2 × 10^9 cells/ml, and treated with recombinant lyticase until most of the cells were converted to spheroplasts. Spheroplasts were collected by low-speed centrifugation and washed twice with 10 mM Tris-HCl (pH 7), 0.7 M sorbitol, 1% glucose and 0.5× SD medium (Dulic *et al*., 1991) with appropriate supplements. The spheroplasts were resuspended to 10^9 spheroplasts/ml. One ml was incubated with 5 nmol of positively charged Nanogold (Nanoprobes, Stony Brook, NY) at 0°C for 15 min and then warmed to 15°C or room temperature before fixing by addition of formaldehyde and glutaraldehyde to final concentrations of 3 and 0.2%, respectively. Spheroplasts were fixed for 2 h at room temperature or overnight at 4°C and washed three times with 50 mM HEPES (pH 7.0) and 3 mM KCl. They were then treated with 1% metaperiodate for 30 min to avoid problems in the embedding procedure caused by the remaining cells that were not converted to spheroplasts (van Tuinen and Riezman, 1987). Dehydration, infiltration, and polymerization in LR Gold resin were as recommended by the supplier (London Resin, London, England). Thin sections of ~50 nm were cut and mounted on nickel grids. Nanogold was enhanced with HQ Silver (Nanoprobes) for 4 min as described by the manufacturer. Sections were then stained with 6% uranyl acetate for 10 min followed by 1 min in lead citrate. The sections were examined with a Philips (Mahwah, NJ) 400 electron microscope at 80 kV. Positively charged Nanogold-labeled structures were quantified on 20 spheroplast profiles for each time point as described (Prescianotto-Baschong and Riezman, 1998).

Fluorescence Microscopy

FHER001-5A cells were transformed with pGFP-TLG2. Transformants were grown to midlogarithmic phase in glucose minimal medium containing 1 mM methionine. The cells were immobilized on poly-L-lysine coated microscope slides, and the slides were mounted with Citifluor (Citifluor, London, England). The fluorescence signal observed after basal transcription was faint and not easily observed with a normal fluorescence microscope. The slides were therefore observed using a computer-assisted image analysis system (Oncor, Gaithersburg, MD), coupled to a cooled, low-level charge-coupled device (CCD) camera (Photometrics, Tucson, AZ), a video CCD camera (C2400, Hamamatsu Photonic Systems, Bridgewater, NY), and an epi-illumination inverted microscope (Axiovert 135, Zeiss, Thornwood, NY). The images were acquired with a plan-apochromat 100, 1.4 oil immersion objective (Zeiss). Transmitted light images were obtained in the differential interference contrast (DIC) mode acquired on the video CCD camera and digitized in a 512 × 474 array on 8 bits. GFP fluorescence images were acquired using the low-level CCD camera and digitized in a 512 × 512 array coded on 16 bits. All images were then exported in 8-bit tagged image file format. NIH Image 1.60 (National Institutes of Health, Bethesda, MD) and Photoshop 4.0 (Adobe Systems, Mountain View, CA) programs were used to make the printed outputs on an Eastman Kodak (Rochester, NY) Colorease printer.

Cells expressing Sec7p-GFP were grown in the dark to log phase. Cells were immobilized on concanavalin A (1 mg/ml)–coated microscope slides, and GFP fluorescence was visualized as described above.

RESULTS

YOL018c Encodes a New Syntaxin Family Member

The product of the YOL018c gene (GenBank accession number Z74760) was first discovered as a relative of Sso2p (Aalto *et al*., 1993) by database search using the BLAST algorithm. Subsequent amino acid sequence comparisons with various t-SNAREs revealed that the C-terminal part (71 residues) upstream of the transmembrane domain (TMD) of the YOL018c-encoded protein is most closely related (35% identity) to the yeast Pep12p, which is essential for transport of some vacuolar hydrolases from the late Golgi to the vacuole (Becherer *et al*., 1996). A recent study by Weimbs *et al*.

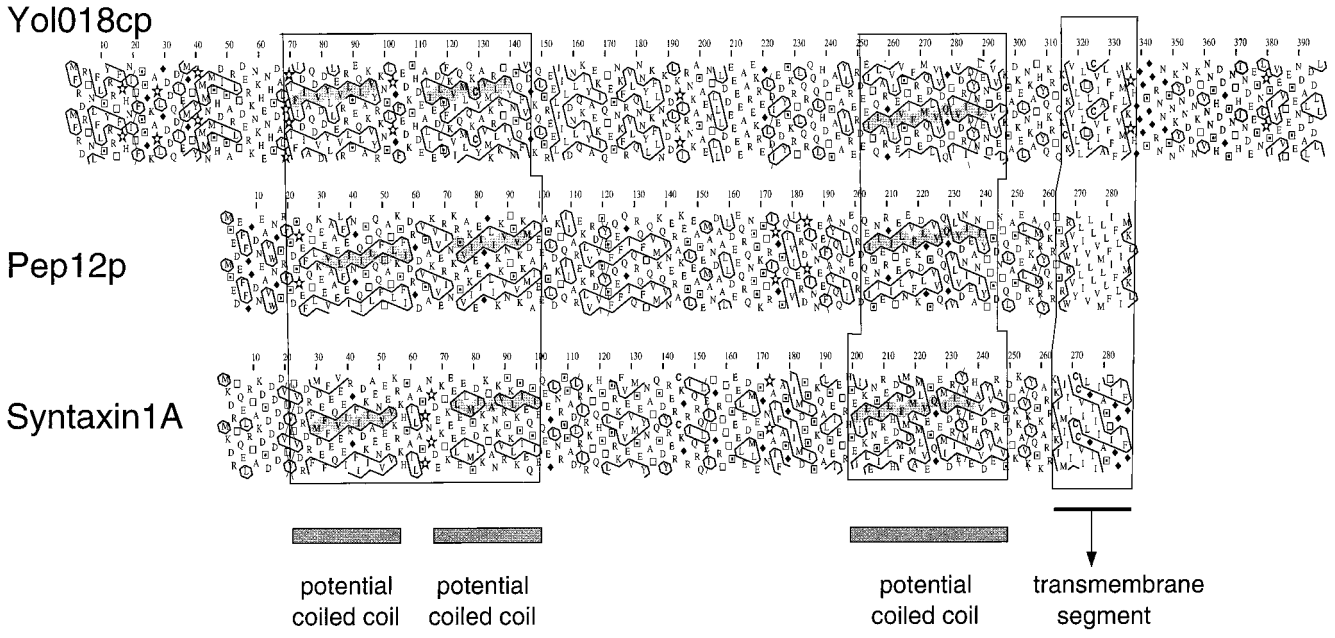

Figure 1. HCA alignments of Yol018cp, Pep12p, and Syntaxin 1A. Boxes indicate the most conserved domains, i.e., putative coiled-coil and transmembrane segments. Residues in gray are those predicted to adopt a coiled-coil conformation. The horizontal shape of the hydrophobic clusters between the domains could indicate the presence of α-helices.

(1997) also identified the protein encoded by YOL018c as a member of the t-SNARE family. This analysis identified a 60-residue domain close to the TMD as the signature of the syntaxin/t-SNARE family, also called the t-SNARE domain. This region is characterized by a heptad repeat, predicted to adopt an α-helical coiled-coil conformation. Considerable progress has been made recently in the understanding of the role of these domains in formation of the SNARE complex (Götte and Fischer von Mollard, 1998).

Proteins of the syntaxin/t-SNARE family are C-terminally anchored, with the bulk of the protein being in the cytoplasm and the coiled-coil domain situated close to the TMD. Some syntaxin family members contain two additional stretches of heptad repeats in their N-terminal region, which could also adopt a coiled-coil conformation (Weimbs *et al*., 1997). YOL018c encodes the longest known member of the yeast syntaxin family with 397 residues (46 kDa), whereas all the others are 280–340 amino acids long.

Secondary structure analysis was carried out using HCA (Callebaut *et al*., 1997) on the YOL018c-encoded protein, its closest homologue yeast Pep12p, and syntaxin 1A, which is the most extensively studied for its interactions with other proteins of the targeting and fusion complex (Figure 1). HCA is a very sensitive method of sequence analysis, its efficiency has been widely demonstrated (Callebaut *et al*., 1997), and it is able to reveal three-dimensional similarities between protein domains showing very limited relatedness at the primary sequence level. This makes it possible to compare secondary structures of proteins according to the shape, distribution, and position of their hydrophobic clusters drawn in two-dimensional representation. HCA revealed that the three t-SNAREs clearly have a similar secondary structure all along the protein. The same was true for all the known yeast t-SNAREs (our unpublished results). This representation highlighted the conserved distribution of the secondary structures, i.e., the three potential coiled-coil domains and the TMD, which are separated by sequences of similar lengths. The YOL018c encoded protein is thus a clear member of the t-SNARE family. Given our observations about the function of this protein in endocytosis, we originally termed this new t-SNARE Tse1p (t-SNARE for endocytosis). Upon completion of this work, Holthuis *et al*. (1998) published a report on the same protein. Thus, we have adopted the name they used, Tlg2p.

Tlg2p is the only known t-SNARE protein that exhibits a C-terminal extension of >60 amino acids after its TMD. To exclude the possibility that this resulted from a sequencing error, the chromosomal gene was isolated and reanalyzed by sequencing. This analysis confirmed the existence of the additional segment, which is predicted to be lumenal and contains three potential glycosylation sites. A tagged protein was obtained by fusing an epitope derived from HA in frame with the Tlg2p N terminus. Extracts were prepared from cells expressing the HA-tagged protein

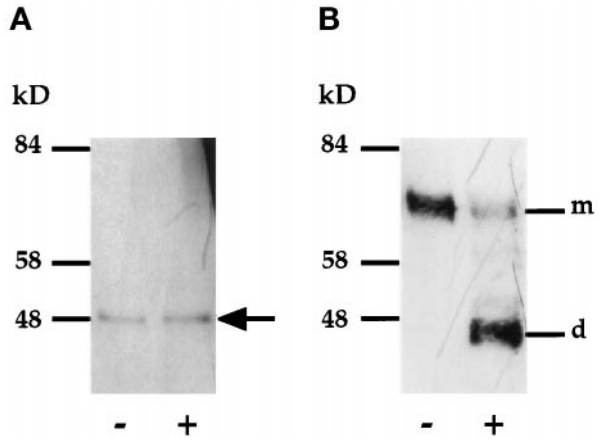

Figure 2. Tlg2p is not glycosylated. FHER001-5A cells transformed with pHA-TLG2 were grown to midlogarithmic phase, and the protein extracts were prepared and incubated in the absence (−) or presence (+) of endoglycosidase H. Extracts were loaded on a 9% polyacrylamide/0.1% SDS gel and analyzed by Western immunoblotting. (A) Detection of HA-Tlg2p (arrowhead). The tagged protein was able to complement the endocytic defect of uracil permease. (B) Detection of CPY. The position of mature CPY (m) or deglycosylated CPY (d) is indicated to the right. Each lane contains proteins extracted from ~6×10^6 cells. Numbers to the left of each panel indicate the position of molecular weight markers loaded onto the same gel.

and analyzed by immunoblot with anti-HA antiserum (Figure 2). A band was detected that migrated as an ~48-kDa protein. This apparent size suggested that Tlg2p is not glycosylated. Protein extracts were treated with endoglycosidase H. No obvious difference in electrophoretic behavior was observed between the immunodetectable protein present in the endoglycosidase H-treated extract and that of the mock-treated sample, whereas a control protein (CPY) was deglycosylated. We conclude that Tlg2p is not glycosylated. The same conclusion was reached by experiments performed using tunicamycin, an inhibitor of N-linked glycosylation (our unpublished results).

TLG2 Is Not an Essential Gene

To determine the function of Tlg2p, the gene was deleted from four different strains, FY1679, W303-BMA64-1B, RH3419, and RH475-8C (Table 1) and replaced by the *KanMX4* marker, a module containing the G418 resistance gene (Wach *et al*., 1994). The deletion was not lethal in any genetic background tested and conferred no obvious growth defect in rich or minimal glucose medium at 30°C. However, a slower growth of the mutant compared with that of parental cells was observed in minimal medium with galactose as a carbon source in either FY1679 genetic background (doubling time of 4 h 15 min and 3 h 30 min for deleted and control cells, respectively) or in W303 genetic background (doubling time of 3 h 25 min compared with 2 h 50 min). The growth of the RH4075 mutant strain was also slightly slower than that of the wild-type strain at 37°C.

TLG2 Exhibits No Genetic Interaction with Known Members of the SEC1 Family

Each t-SNARE has been shown to interact genetically or physically with a given member of the Sec1p family that functions at the same vesicle targeting and fusion step. Genetic interaction between *TLG2* and known members of the *SEC1* family was studied by crossing the *sly1* (Ossig *et al*., 1991), *sec1* (Novick and Schekman, 1979), *vps45* (Cowles *et al*., 1994), or *slp1/vps33* (Wada *et al*., 1990) temperature-sensitive mutant strains with the *tlg2*Δ strain and testing the viability of the double-mutant haploids after tetrad analysis. No indication of synthetic lethality or of any other phenotype could be detected in double mutants. Moreover, overexpression of *TLG2* from pHA-TLG2 could not suppress the growth defect in the *sly1, sec1*, or *slp1/vps33* temperature-sensitive mutants. Therefore, *TLG2* exhibits no genetic interaction with known members of the *SEC1* gene family.

*The Secretory Pathway Is Not Impaired in tlg2*Δ

t-SNAREs could potentially act on the secretory or endocytic pathway. Most of the genes involved in the secretory pathway are essential genes, which is not the case for genes involved either in Golgi to vacuole targeting or in endocytosis (Klionsky *et al*., 1990; Riezman, 1993). To determine whether Tlg2p is involved in secretion, we monitored the intracellular fate of a marker of the secretory pathway, uracil permease, encoded by the *FUR4* gene. Plasma membrane delivery of uracil permease can be followed by measuring the increase in uracil permease activity that becomes detectable shortly after induction of its synthesis (Moreau *et al*., 1997). To do this, wild-type and *tlg2*Δ cells were transformed with a multicopy plasmid encoding the *FUR4* gene under the control of the *GAL10* promoter. Permease synthesis was induced by the addition of galactose. Uracil permease activity appeared 20 min after induction, with identical kinetics in wild-type and *tlg2*Δ cells (Figure 3A), indicating that the overall secretory pathway was apparently not impaired in *tlg2*Δ cells. In agreement with this result, we observed unchanged electrophoretic patterns for other markers of the secretory pathway, such as the O-glycosylated GPI-anchored protein Gas1p or the heavily mannosylated invertase and acid phosphatase (our unpublished results).

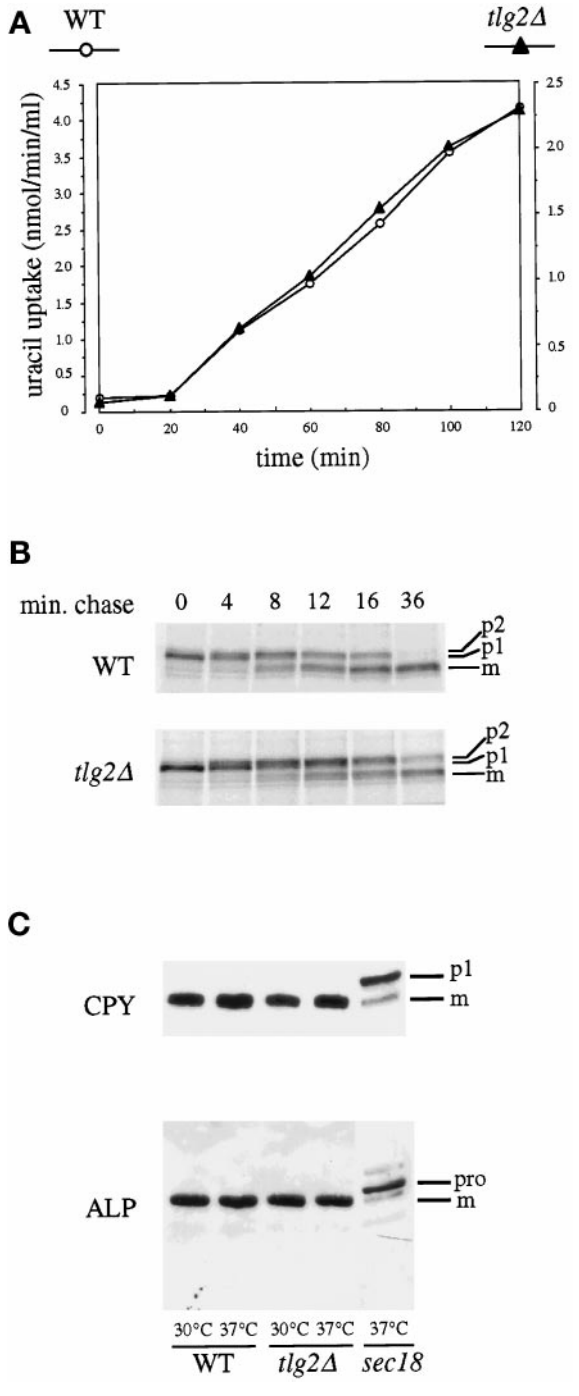

Figure 3. (A) The overall secretory pathway is not impaired in *tlg2*Δ cells. FHER001-3B (WT) and FHER001-5A (*tlg2*Δ) transformed by p195gF (2μ *URA3 GAL-FUR4*) were grown in 2% lactate minimal medium to an A_{600} of 0.4. Galactose (4%) was added to induce uracil permease expression. Uracil uptake activity was measured at various time intervals. The lower uracil permease specific activity in mutant relative to wild-type cells accompanied by a parallel lower amount of immunodetected permease probably resulted from the slower growth of these cells in galactose medium. Transformation of disrupted cells with centromeric plasmid carrying *TLG2* complemented the slower growth and the reduction in permease

*tlg2*Δ *Is Synthetically Lethal with vma2*Δ

Many mutants that are defective in endocytosis in yeast show synthetic lethality with mutants in the vacuolar H^+-ATPase (*vma2*Δ, for example). This has been suggested to be due to simultaneous disruption of vacuolar acidification and fluid phase endocytosis required to acidify the endocytic pathway (Munn and Riezman, 1994). A *vma2*Δ strain (RH3419), which contains a mutation in the *VMA2* gene and a plasmid carrying both the *VMA2* and *URA3* genes, was transformed with the *TLG2* disruption cassette containing *KanMX4*. Three transformants that grew on G418 were submitted to PCR amplification of the *TLG2* genomic region: transformants 1 and 2 contained a disrupted *TLG2* locus, whereas transformant 3 showed a normal *TLG2* gene. The three transformants were streaked onto plates containing 5-fluoroorotic acid to cure the plasmid carrying the *URA3* and *VMA2* genes. The two verified disruptants did not grow on 5-fluoroorotic acid plates, whereas the *vma2*Δ strain with a wild-type *TLG2* locus grew normally. Consequently, the *tlg2*Δ mutation is synthetically lethal with *vma2*Δ. Normally after several days growth on plates with a limiting amount of adenine, *ade2* cells become deep red. We found that the *tlg2*Δ *ade2* cells were pink rather than red, a property that is also characteristic of endocytosis mutants and other mutants that affect vacuolar functions (Riezman, unpublished observations). Based on these results it is likely that deletion of Tlg2p affects endocytosis.

*tlg2*Δ *Cells Are Impaired in Endocytosis in a Step Subsequent to Internalization*

Wild-type and *tlg2*Δ strains were examined for their ability to internalize and degrade α-factor. This pheromone is a useful endocytic marker in yeast because one can measure its internalization independently from its subsequent degradation, which normally takes place in the vacuole (Riezman *et al*., 1996). The kinetics of internalization of radiolabeled α-factor by

Figure 3 (cont). (our unpublished results). (B and C) Maturation of vacuolar proteins CPY and and ALP in wild-type and *tlg2*Δ cells. (B) FHER001-3B (WT) and FHER001–5A (*tlg2*Δ) cells were pulse labeled with [^{35}S]methionine and chased with nonradioactive methionine for the indicated times. CPY was immunoprecipitated from samples taken at various times. The immunoprecipitates were analyzed on 7.5% polyacrylamide/0.1% SDS gels and visualized by fluorography. p1, ER form; p2, Golgi form; m, mature vacuolar form. (C) FHER001-3B (WT), FHER001-5A (*tlg2*Δ), and SL (*sec18*) cells were collected in the exponential phase in YPD medium at 30°C (24°C for SL) and either left at permissive temperature or transferred to 37°C for 2 h. Protein extracts were prepared. Aliquots corresponding to 4×10^6 cells were analyzed for CPY and ALP by Western immunoblotting. In *sec18* cells, mature proteins synthesized before the temperature block, and ER-accumulated forms of CPY (p1) and ALP (pro) synthesized after exposure at the restrictive temperature, were visible.

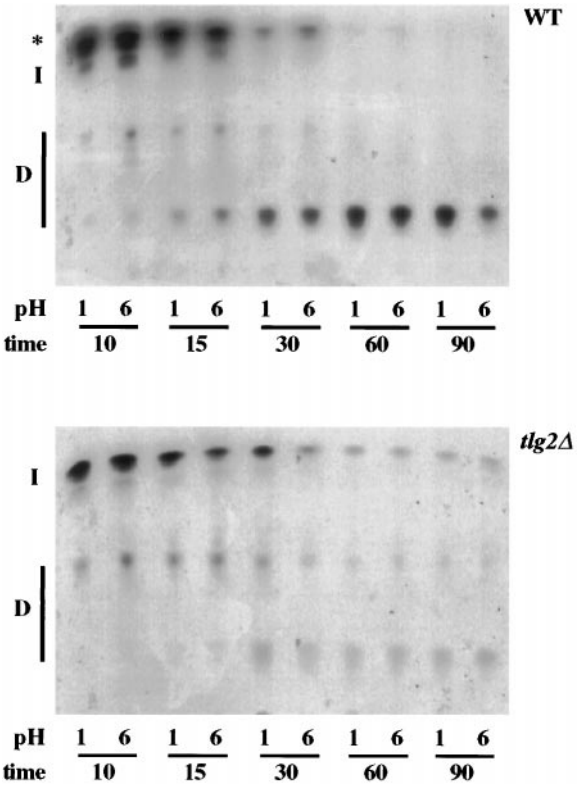

Figure 4. Degradation of α-factor. RH475-8C (WT) and RH4075 (*tlg2*Δ) cells were grown overnight, washed, and incubated with [^{35}S]α-factor at 0°C, washed again, and then resuspended in 30°C rich medium. At the indicated times the cells were washed with pH 1 (to remove surface bound pheromone) or pH 6 buffers and collected on filters. The cells were extracted, and extracts were analyzed by thin layer chromatography. I, Intact α-factor; D, degradation products; *, smear near the intact α-factor, which is one of the primary degradation products.

*tlg2*Δ cells (strain RH4074) and isogenic wild-type cells (strain RH475-8C) were measured. Both strains showed rapid and identical α-factor internalization at 30°C ($t_{1/2}$ = 7.5 min). We next measured α-factor degradation in the same two strains at 30°C (Figure 4). Cells were incubated with radiolabeled α-factor, and at various times the pheromone was extracted and analyzed by TLC and fluorography. In wild-type cells, one of the earliest events in α-factor degradation is the appearance of a smear that runs near the intact pheromone (Wichman *et al*., 1992). This smear was seen in wild-type cells but not in the *tlg2*Δ mutant. In wild-type cells, α-factor was almost completely degraded by 60 min, and degradation products were prominent. In *tlg2*Δ cells some of the α-factor remained intact throughout the assay, and the degradation products appeared less intense. These data indicated that the *tlg2*Δ cells show a delay in α-factor degradation.

Measuring clearance of transporters from the plasma membrane under conditions that trigger their internalization provides another sensitive way to follow endocytosis. Uracil permease undergoes rapid internalization followed by vacuolar degradation in cells submitted to various stress conditions, such as inhibition of protein synthesis (Volland *et al*., 1994). After addition of cycloheximide, the fate of uracil permease was compared in wild-type and *tlg2*Δ cells (FY1679 genetic background) overexpressing the uracil permease. Uracil uptake was measured at various times, providing an accurate index of plasma membrane–located permease. Protein extracts were prepared in parallel and analyzed for uracil permease by Western immunoblotting. Wild-type and disrupted cells exhibited a similar time-dependent loss of uracil uptake (Figure 5A), indicating that the disruption did not inhibit permease internalization. This process was even slightly accelerated in *tlg2*Δ cells ($t_{1/2}$ = 20 min vs. 28 min for wild-type cells). The same observation was made in another genetic background (W303 cells), showing that the defect resulted from the deletion of *TLG2* (Figure 5C). Furthermore, this slight acceleration of internalization disappeared after expression of *TLG2* from a centromeric plasmid in *tlg2*Δ cells. If internalization of uracil permease was not delayed in *tlg2*Δ cells, the rate of permease degradation was strongly reduced in *tlg2*Δ cells (Figure 5B). The pool of permease originally present in wild-type cells was noticeably degraded by 30 min and had almost completely disappeared in 2 h. In contrast, much less degradation was observed in *tlg2*Δ cells, which still exhibited a strong permease signal 2 h after addition of cycloheximide. By serial dilution of the protein extracts we estimated that the $t_{1/2}$ of permease degradation was increased more than twofold in *tlg2*Δ cells compared with the wild type. The same observations were made in another genetic background (Figure 5D). Trafficking of the permease to the vacuole was therefore significantly slowed down in the *tlg2*Δ cells.

The degradation phenotypes observed in *tlg2*Δ cells indicate that the endocytic pathway is perturbed in these cells, because the vacuolar hydrolases that are responsible for α-factor and uracil permease degradation are formed at nearly normal levels in the mutant cells (see below). *TLG2,* which is not required for the internalization step, is involved in one of the subsequent steps of endocytosis, such as delivery to early endosomes, late endosomes, or the vacuole.

Biosynthetic Vacuolar Delivery Is Almost Normal in tlg2Δ Cells

The yeast vacuole receives material from two vesicular pathways: biosynthetic trafficking from the Golgi apparatus and endocytic trafficking from the cell surface. These two pathways converge at an endosomal compartment. Delivery from endosomes to the vacuole can be easily checked by following the traffic of pro-

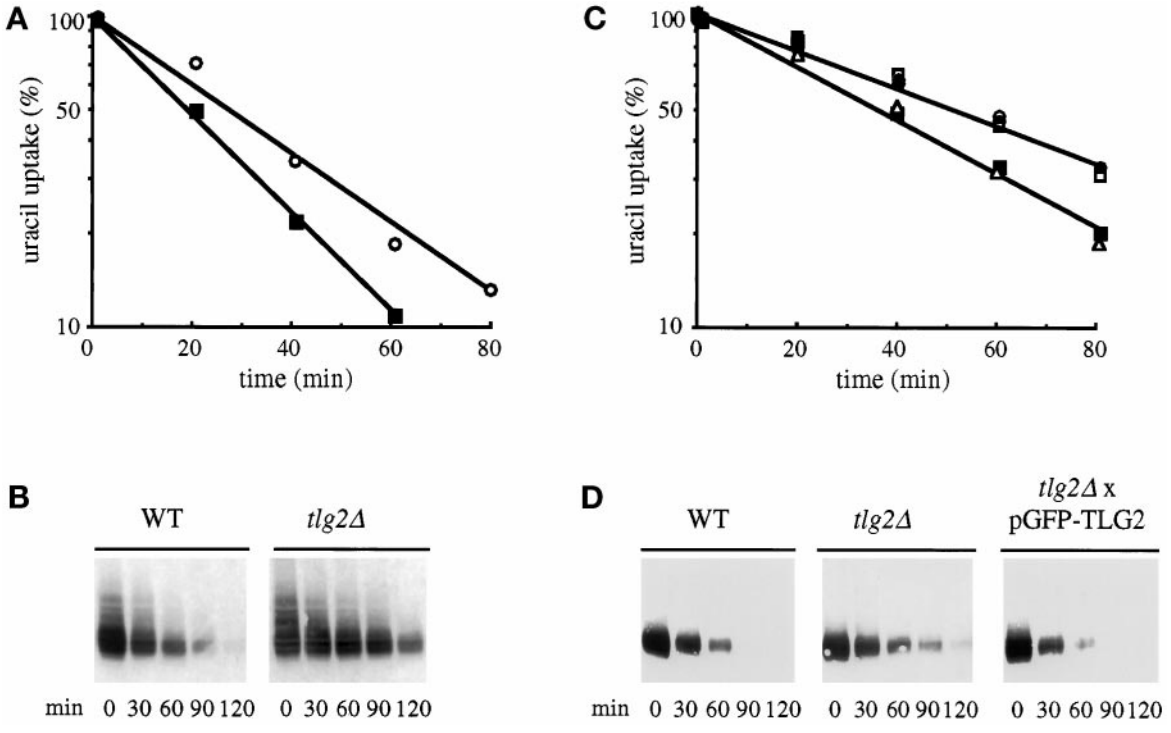

Figure 5. Degradation of uracil permease is impaired in *tlg2*Δ cells. (A and B). FHER001-3B and FHER001-5A strains (respectively indicated as WT and *tlg2*Δ) transformed with the plasmid p195gF (2μ *URA3 GAL-FUR4*) were grown at 30°C to an A_{600} of 0.6 with galactose as a carbon source. They were transferred to 37°C. Fifteen minutes later cycloheximide (100 μg/ml) was added. (A) Uracil permease activity (uptake) was measured at different times after the addition of cycloheximide. The results are expressed as percent of initial activities. ○, Wild type; ■, *tlg2*Δ. (B) Protein extracts were prepared at the times indicated after the addition of cycloheximide. Aliquots were analyzed for uracil permease by Western immunoblotting. Volumes corresponding to 0.2 and 0.3 ml of culture were analyzed for wild-type and *tlg2*Δ cells, respectively, to compensate for lower amounts of permease in disrupted cells. Permease appeared as several bands corresponding to the various phosphorylated states (Volland *et al*., 1994). Bands sometimes detected in total extracts above the main permease signal correspond to ubiquitin–permease conjugates, more readily detectable on membrane-enriched fractions (Galan *et al*., 1996). (C and D). The same experiment was performed in another genetic background at 30°C, a temperature that resulted in sufficiently rapid endocytosis in W303 cells. W303-BMA64-1B or WHER006-03B strains cotransformed with the plasmids pgF (2μ *LEU2 GAL-FUR4*) and pFL38 (CEN/ARS *URA3*) (respectively indicated as WT and *tlg2*Δ) or pgF and pYCG-YOL018c (CEN/ARS *URA3 TLG2*; indicated as *tlg2*Δ × pTLG2) or pgF and pGFP-TLG2 (CEN6/ARSH4 *URA3 GFP-TLG2*; indicated as *tlg2*Δ × pGFP-TLG2) were grown as described above. In the latter case, growth was performed in the absence (C) or presence (C and D) of 1 mM methionine. Cycloheximide (100 μg/ml) was added. (C) At different times, uracil uptake was measured. ○, Wild type; ■, *tlg2*Δ; □, *tlg2*Δ × pTLG2; △ and ●, *tlg2*Δ × pGFP-TLG2 under conditions of basal expression (△) and overexpression (●). (D) Protein extracts were prepared at the times indicated after the addition of cycloheximide, and aliquots were analyzed for uracil permease by Western immunoblotting as described above. Overexpressed GFP-tagged Tlg2p reestablished wild-type permease amounts and internalization rates. Basal expression of GFP-Tlg2p partially reestablished wild-type permease amounts but not wild-type permease internalization.

teins destined to the vacuole. Wild-type and *tlg2*Δ cells were analyzed for their ability to process CPY. This vacuolar hydrolase is a soluble glycosylated protein that undergoes processing from a core-glycosylated ER form (p1) to a modified Golgi form (p2) before being proteolytically cleaved in the vacuole to the mature species. Figure 3B shows a pulse–chase experiment performed on the wild-type and *tlg2*Δ strains. Processing from p1 to p2 occurred similarly in the wild-type and *tlg2*Δ strains, confirming that transit from the ER to the Golgi is normal in *tlg2*Δ cells. However, processing of p2 to mature CPY appeared slightly delayed in the mutant compared with the wild-type cells. Analysis by Western immunoblotting of total protein extracts revealed no accumulation of the p2 form (Figure 3C) and identical steady-state levels of the mature CPY form. Thus, the traffic of CPY from the Golgi to the vacuole is almost normal in *tlg2*Δ cells. Alternative pathways for the sorting of either soluble or membrane-bound vacuolar proteins have been reported (Jones *et al*., 1997). We therefore tested the fate of other vacuolar markers in *tlg2*Δ cells. The transport of a second soluble vacuolar marker, proteinase A, was not affected in mutant cells compared with wild-type cells, as indicated by pulse–chase experiments. Processing of the membrane-bound ALP was also checked by Western immunoblotting of total protein extracts (Figure 3C). Only the mature ALP

form was detected in *tlg2*Δ cell extract as in wild-type cell extracts, indicating that ALP was matured normally. Moreover, the steady-state levels of the mature form of ALP were identical in wild-type and *tlg2*Δ cells (Figure 3C). Taken together, these observations indicate that several proteins are efficiently targeted from the Golgi to the vacuole in the absence of Tlg2p function.

The TLG2 Gene Product Is Required for the Biogenesis of Normal Endosomal Structures

*tlg2*Δ cells did not present gross morphological changes, apart from slightly more fragmented vacuoles than those in wild-type cells. The only clear effect of *TLG2* deletion was a significant accumulation in >25% of the cells of small vesicles (Figure 6A) of ~50–70 nm in diameter located predominantly at the periphery of the cells (Figure 6B). To identify the nature of these vesicles, and more generally to visualize the endocytic pathway in wild-type and *tlg2*Δ cells, spheroplasts derived from RH475–8C and RH4074 were incubated with positively charged Nanogold, which has recently been developed as an endocytic tracer and which can be visualized in the electron microscope (Prescianotto-Baschong and Riezman, 1998). Using this technique, gold particles are sequentially detected in primary endocytic vesicles, early endosomes, late endosomes, and vacuoles. Spheroplasts were incubated with Nanogold and then fixed, and thin sections were cut. Nanogold (which has a diameter of <1 nm) was visualized after enhancement with HQ Silver. Several different intracellular structures could be visualized in wild-type spheroplasts after 15 min of incubation at room temperature (Figure 7, A and B). An extensive tubular–vesicular structure defined as an early endosome (Figure 7B) as well as a relatively large (~200 nm) oval structure corresponding to a late endosome (Figure 7A; Prescianotto-Baschong and Riezman, 1998) were observed. Some labeling was visible in vacuoles. The structures seen in the *tlg2*Δ cells at this time point were very different (Figure 7C–H). The Nanogold was mainly found in small vesicular structures likely corresponding to primary endocytic vesicles, and no labelling was visible in the vacuole. By 40 min, Nanogold was seen in both strains over vacuoles, indicating that the endocytic content can reach the vacuole in wild-type and *tlg2*Δ cells (our unpublished results). Both strains also showed strong labeling in late endosomes, but still no well-developed early endosomal structures were found in the *tlg2*Δ cells even though a few structures resembling this organelle were visible (Figure 7I). In general, much of the label found in early endosomal structures in wild-type cells was seen in tubular structures (Figure 7B; Prescianotto-Baschong and Riezman, 1998), but in the structures resembling early endosomes in *tlg2*Δ cells most of the labeling was seen in vesicular structures (Figure 7I). To analyze the endo-

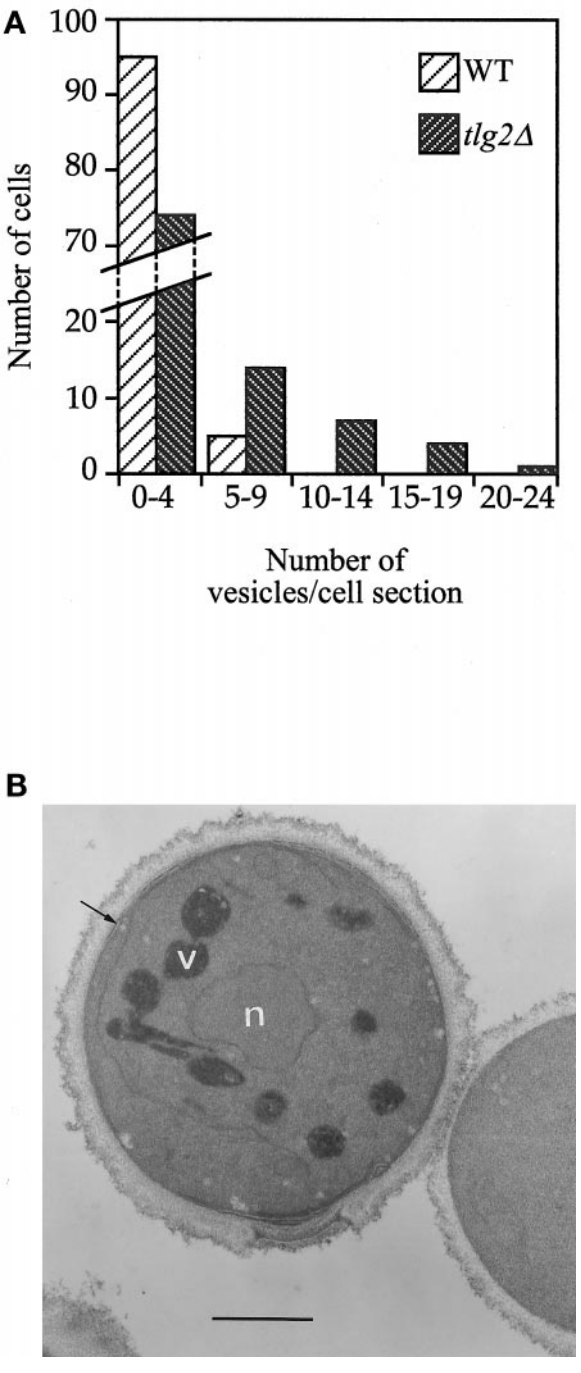

Figure 6. Accumulation of vesicles in *tlg2*Δ cells. Wild-type and *tlg2*Δ cells were grown to midlogarithmic phase in YPD medium at 30°C. Intact cells were fixed with glutaraldehyde, stained with $KMnO_4$, embedded, and sectioned as described by Goodson *et al*. (1996). (A) The numbers of vesicles per cell section were counted in 100 cells. (B) A typical *tlg2*Δ cell with accumulated vesicles, indicated by the arrows. N, Nucleus; V, vacuoles. Bar, 1 μm.

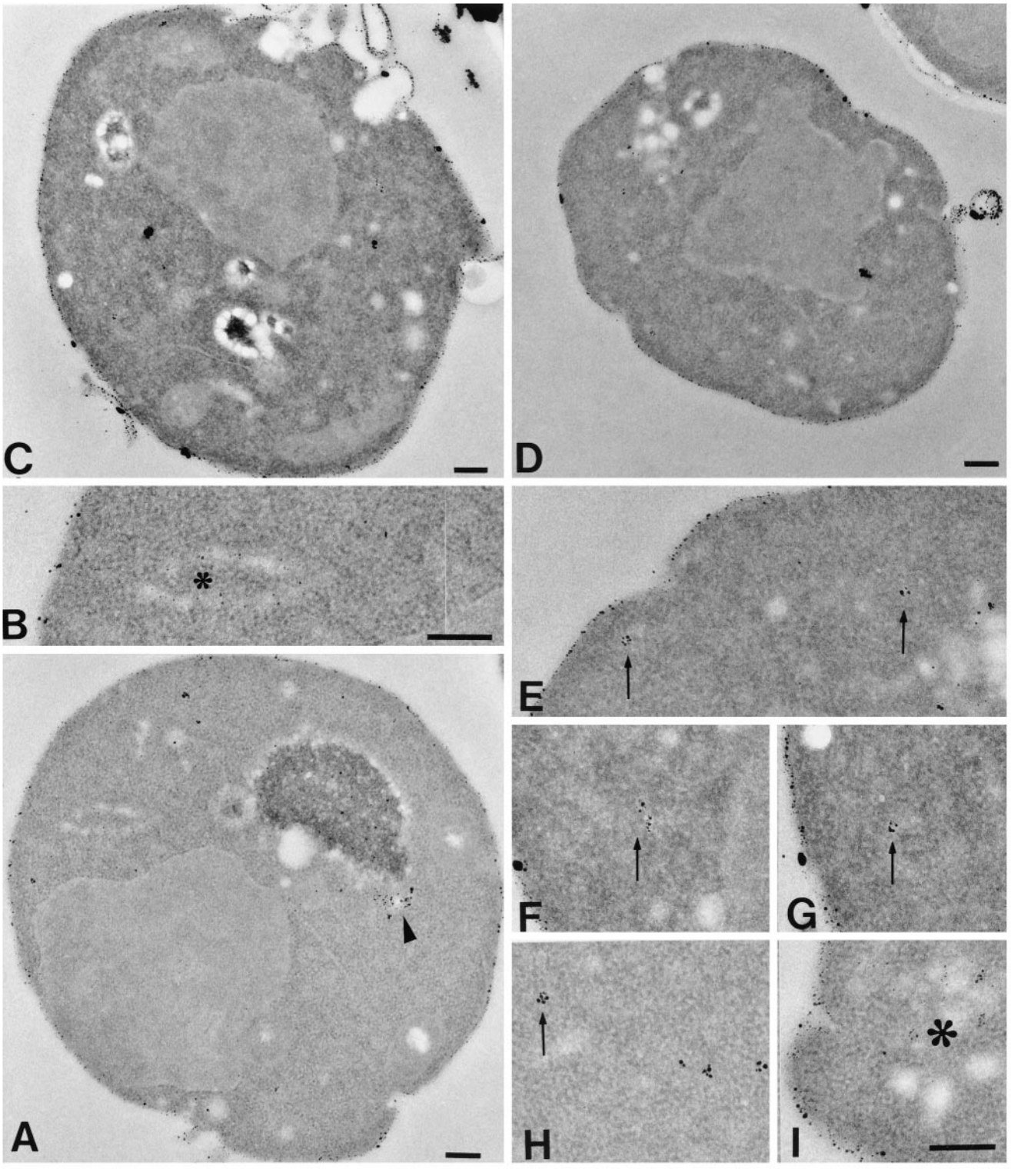

Figure 7. Internalization of positively charged Nanogold. Wild-type (A and B) and *tlg2*Δ (C–I) spheroplasts were incubated with positively charged Nanogold on ice for 5 min and then shifted to room temperature for 15 min. The cells were fixed, dehydrated, and embedded. Thin sections were generated and enhanced with HQ Silver and visualized in the electron microscope. Endocytic vesicles found in *tlg2*Δ cells are labeled with arrows; an early endosome from wild-type cells is labeled with an asterisk, as is a structure from *tlg2*Δ cells, which resembles an early endosome somewhat. The triangle in A indicates late endosomes. Bar, 200 nm.

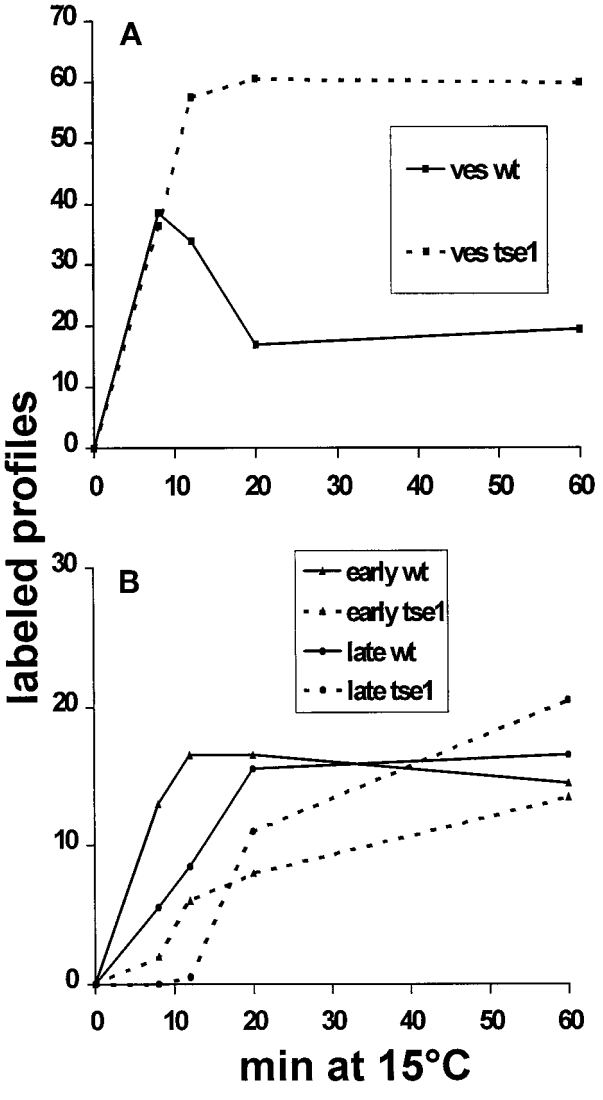

Figure 8. Quantitation of Nanogold-labeled structures. Wild-type and *tlg2*Δ spheroplasts were incubated with positively charged Nanogold on ice for 5 min and then shifted to 15°C for various times up to 60 min. The cells were fixed, dehydrated, and embedded. Thin sections were generated and enhanced with HQ Silver and visualized in the electron microscope. Labeled vesicles, early endosomes, and late endosomes were identified on sections and quantified. The vesicle quantitation is shown in A, the early and late endosome quantitation in B.

cytic defect quantitatively by this technique, we performed a time course of incubation of yeast spheroplasts at 15°C, a temperature at which the transport rate through endosomes is differentially decreased, and incubated for various times before fixation. The samples were processed as above, and the labeled vesicles, early endosomes, and late endosomes were quantified (Prescianotto-Baschong and Riezman, 1998). It is clear that the number of labeled small endocytic vesicles continued to increase with incubation time in the *tlg2*Δ mutant (Figure 8A), whereas in wild-type cells their number began to decline after 8 min. In addition, few early endosomal structures were detectable in the mutant cells at early time points. At late time points there was some labeling of structures resembling early endosomes in the *tlg2*Δ mutant, but with this additional time the label could have made its way to the Golgi, which has a similar morphology to early endosomes. The appearance of late endosome labeling was delayed in the mutant cells (Figure 8B). These results are consistent with the delay seen in the processing of various endocytic markers and suggest that the *TLG2* gene may be required for biogenesis of normal early endosomal structures even though this gene is not absolutely required for delivery of endocytic content to the vacuole.

GFP-tagged Tlg2p Is Localized at the Periphery of the Cell

To obtain some information about the localization of Tlg2p, the protein was tagged at its N terminus with the GFP, and the GFP-tagged gene was cloned in a centromeric plasmid. The expression of the tagged protein was under the control of the regulatable *MET25* promoter, which allows basal transcription of the gene in the presence of 1 mM methionine (Mumberg *et al*., 1994). Expression of the tagged protein in either the presence or absence of methionine complemented the slight growth delay, as well as the uracil permease endocytic degradation defect (Figure 5D and our unpublished results). Because overexpression of t-SNAREs is thought to result in possible mislocalization (Götte and Fischer von Mollard, 1998), we checked the localization of GFP-tagged Tlg2p under conditions of basal expression. Expression at the basal level of the GFP-tagged Tlg2p in *tlg2*Δ cells was so low that it could not be detected with an ordinary fluorescence microscope, but the signal became visible with a computer-assisted image analysis system. GFP-tagged Tlg2p showed a unique pattern, almost always consisting of small structures at the periphery of the cell, apparently under the plasma membrane and distant from the vacuoles as vizualized by DIC optics (Figure 9). No staining was observed that might correspond to plasma membranes, ER, or vacuoles, all of which give easily identified immunofluorescence images. No juxtavacuolar staining was observed as described for the late endosome/prevacuolar compartment (Davis *et al*., 1993). The distribution of Tlg2p also appeared distinct from that reported for the Golgi, which appears as heterogeneous punctate structures distributed throughout the cytoplasm when visualized by immunofluorescence using antibodies against Golgi markers such as Sec7p (Franzusoff *et al*., 1991). To confirm that the difference in localization pattern between Tlg2p and Sec7p is not due to a difference in method-

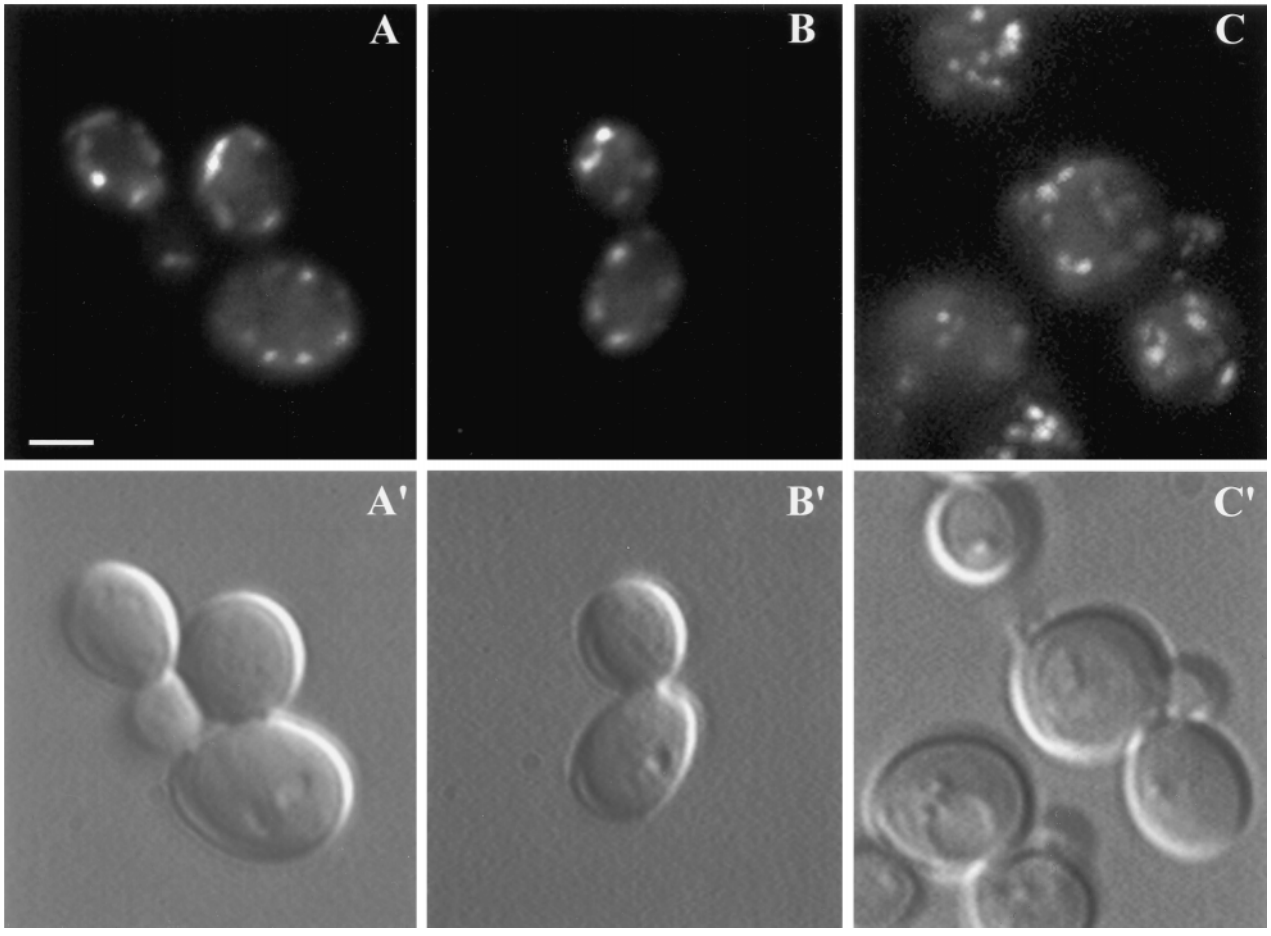

Figure 9. Localization of GFP-tagged Tlg2p and Sec7p. Fluorescence of GFP-tagged Tlg2p in the presence of 1 mM methionine is shown to the left (A and B), and fluorescence of GFP-tagged Sec7p is shown to the right (C); the corresponding cells visualized with DIC optics are shown below (A′–C′). In cells expressing GFP-tagged Tlg2p, the fluorescence is located in small structures at the periphery of the cells, not linked with the vacuole. Twenty-seven of 35 cells observed presented the same fluorescence pattern. In cells expressing GFP-tagged Sec7p, the fluorescence is located in punctate structures throughout the cytoplasm. All the cells observed (33) presented the same pattern. Bar, 2.5 μm.

ology, we created a GFP-tagged version of Sec7p and analyzed its distribution by fluorescence microscopy. Indeed, GFP-tagged Sec7p gives a typical Golgi staining pattern, namely, punctate structures localized throughout the cytoplasm rather than immediately underlying the plasma membrane. The fluorescence pattern of GFP-tagged Tlg2p is reminiscent of the immunofluorescence pattern observed for the Ste2p receptor at early times after α-factor-induced endocytosis (Hicke *et al*., 1997). Therefore, GFP-tagged Tlg2p is probably not primarily localized in the Golgi but more likely in early endosomes under conditions of basal expression.

DISCUSSION

The results presented strongly suggest that Tlg2p, a member of the t-SNARE family, functions at an early step of the endocytic pathway subsequent to internalization, probably at the level of early endosomes.

Apart from its general structural organization, typical of a t-SNARE, two features of Tlg2p deserve special attention. The predicted TMD of Tlg2p is 18 amino acids long. Recent data indicate that long TMDs (~25 amino acids) would play a critical role in plasma membrane localization, whereas for shorter TMDs less easily definable physical properties, including amino acid composition or cytosolic signals, would be important to define ER/Golgi or endosome/vacuolar localization (Rayner and Pelham, 1997). The intracellular localization of Tlg2p is in agreement with the short length of its TMD. Various cytosolic signals have been described to play a role in determining the localization of integral membrane proteins to various subcompartments of the secretory/vacuolar pathways. The predicted cytoplasmic domain of Tlg2p exhibits neither

KKXX sequences nor Tyr- and/or Phe-based sequences known to be, at least for some proteins, key features of ER or Golgi localization signals (Wilcox *et al*., 1992). Interestingly, Tlg2p is the only t-SNARE identified to date that possesses a substantial predicted lumenal domain. Abeliovich *et al.* (1998) indeed demonstrated the lumenal orientation of this domain. Three potential glycosylation sites are present in this domain. They are predicted to lie at 12, 22, and 26 amino acids dowstream of the TMD, distances that should allow accessibility of two of these sites to the oligosaccharyl transferase (Nilsson *et al*., 1994). However, surprisingly, an N-terminally HA-tagged version of the protein is not glycosylated. The function, if any, of the C-terminal lumenal extension of Tlg2p remains to be demonstrated, inasmuch as it was found to be dispensable for complementing some defects associated with deletion of *TLG2* (Abeliovich *et al*., 1998).

We found no involvement of Tlg2p in the secretory pathway, as evidenced by normal targeting of uracil permease to the plasma membrane and normal processing of Gas1p, acid phosphatase, and invertase in *tlg2*Δ cells. In contrast, the finding that the deletion of *TLG2* is synthetically lethal with *vma2*Δ suggests a role of *TLG2* in endocytosis. The search for mutants unable to lose a plasmid uncovering the *VMA2* deletion led to the identification of several *end* mutants (Munn and Riezman, 1994), affected either at the internalization step or at subsequent steps of the endocytic pathway (namely, delivery from endosome to vacuole). The present report constitutes the first use of the synthetic lethality with *vma2*Δ to identify the involvement in endocytosis of a given gene. The involvement of Tlg2p in endocytosis was confirmed in *tlg2*Δ cells by following the fate of two established endocytic markers, α-factor and uracil permease, and that of a recently introduced endocytic tracer, positively charged Nanogold. In all three cases, internalization proceeded normally. However, degradation of α-factor and uracil permease was delayed. Both proteins did reach either the late endosome or the vacuole in *tlg2*Δ cells (it has been demonstrated that some degradation can occur in the late endosomes; Schimmöller and Riezman, 1993) but less rapidly than in wild-type cells. Involvement of Tlg2p in endocytosis was also supported by the observation in *tlg2*Δ cells of reduced uptake of lucifer yellow and reduction in the rate of ligand-induced degradation of Ste3p (Abeliovich *et al*., 1998) and Ste2p (Holthuis *et al*., 1998).

Using electron microscopy to follow the fate of Nanogold particles internalized by endocytosis allowed more precise identification of the endocytic step impaired in *tlg2*Δ cells. Structures typical of late endosomes and vacuoles are clearly still present in the mutant, even though the vacuoles are more fragmented than in wild-type cells. In contrast, the structure of early endosomes is severely impaired in *tlg2*Δ cells. Early endosomes have been described in mammalian cells (Gruenberg and Maxfield, 1995) and more recently in yeast (Prescianotto-Baschong and Riezman, 1998), as tubular–vesicular structures at the periphery of the cells. These structures are significantly less developed in the *tlg2*Δ mutant. Nanogold particles, found much less frequently in early endosomal-type structures in the mutant, exhibited a pronounced accumulation in small vesicles soon after internalization. Interestingly, very similar vesicles accumulate in *sec18-1* cells at the restrictive temperature (Prescianotto-Baschong and Riezman, 1998). It seems likely that these vesicles show a reduced ability to fuse to form early endosomes in *tlg2*Δ cells. Nevertheless, Nanogold particles were able to reach late endosomes after a significant delay and were ultimately found in vacuoles. This indicates that delivery to late endosomes was probably not affected and that the tracer could bypass early endosomes to reach late endosomes and vacuoles in *tlg2*Δ cells. The same is probably true for the two endocytic markers, which were both ultimately degraded, although more slowly in *tlg2*Δ cells than in wild-type cells. We propose that Tlg2p is required for the biogenesis of normal early endosomes. Tlg2p would be involved at the same step as Sec18p, i.e., plasma membrane to early endosome. We suggest in addition that an early step of the endocytic pathway can be bypassed by direct fusion between primary endocytic vesicles and late endosomes.

A localization of Tlg2p in early endosomes would be consistent with our hypothesis of a role of Tlg2p in the biogenesis of this compartment. An N-terminally GFP-tagged Tlg2p that was able to complement the endocytic defect of *tlg2*Δ cells was visualized in structures at the periphery of intact cells, a pattern that might correspond to early endosomes. This pattern was clearly distinct from that observed for a GFP-tagged version of the late Golgi marker Sec7p, which gave punctate structures throughout the cell. However, based on fractionation on sucrose gradients, and immunofluorescence data using C-terminally tagged proteins, Holthuis *et al*. (1998) proposed that Tlg2p (for t-SNARE of late Golgi) is primarily located in the late Golgi, whereas another t-SNARE, Tlg1p, would be located in early endosomes. But the sucrose gradients described gave poor discrimination between Golgi and endosomes, and it is unlikely that early and late endosomes were separated under these conditions. When Tlg2p was overexpressed under the control of a strong promoter, it partially colocalized (as judged by immunofluorescence) with the late Golgi marker Kex2p. Interestingly, however, images showing Tlg2p expressed from its endogenous promoter were rather different, clearly distinct from that of the early Golgi marker Sed5p (Holthuis *et al*., 1998) and very similar to the peripheral localization we have observed. Abe-

liovich *et al.* (1998) suggested that Tlg2p might indeed be localized in endocytic structures, which according to their data would correspond to late endosomes. Clearly, additional localization experiments coupled with internalization of endocytic markers are needed for definitive localization of untagged Tlg2p. Although several markers of the late Golgi have been characterized, markers of early endosomes remain elusive. Early endosomes are not yet a well-defined compartment in yeast. First identified by fractionation techniques based on the use of Nycodenz gradients (Singer-Krüger *et al*., 1993), early endosomes have been more recently visualized by immunofluorescence as small punctate structures at the periphery of the cell at early times after internalization of either the vital dye FM4-64 (Vida and Emr, 1995) or the Ste2p receptor (Hicke *et al*., 1997), and by electron microscopy as tubular–vesicular structures (Prescianotto-Baschong and Riezman, 1998). Our data suggesting that Tlg2p is located in early endosomes are compatible with the overall endocytic defect observed in *tlg2*Δ cells, with the accumulation of Nanogold particles in primary endocytic vesicles and with the absence of early endosomes visualized by electron microscopy in these cells.

No strong defect of vacuolar protein targeting was detected in the *tlg2*Δ cells. CPY and ALP, which are targeted to the vacuole by two parallel pathways (Cowles *et al*., 1997), are processed almost normally and found in normal steady-state amounts in *tlg2*Δ cells. In agreement with these data, no synthetic lethality was observed between *tlg2*Δ and either *vps45* or *slp1/vps33,* strains impaired in genes encoding proteins of the *SEC1* family that are involved in the traffic from Golgi to prevacuolar compartment, or from prevacuolar compartment to vacuole, respectively. Taken together, these data and our results with the positively charged Nanogold imply that the late endosome to vacuole step was not affected in *tlg2*Δ mutant cells. It is possible that the short delay observed in CPY maturation might be due to abnormal targeting of late Golgi-derived vesicles that would normally fuse with an early endocytic compartment (i.e., early endosomes), as is the case in mammalian cells (Robinson *et al*., 1996) and as already suggested for *ypt51*Δ cells (Singer-Krüger *et al*., 1995). In *tlg2*Δ cells, these vesicles could be diverted directly to late endosomes as may be the case for the incoming endocytic vesicles that were seen in the mutant.

t-SNAREs are thought to define subcellular compartments by selecting the incoming vesicles (Hay and Scheller, 1997). This idea would be compatible with our hypothesis that Tlg2p is on early endosomes and our finding that the early endosomal compartment is severely disrupted in *tlg2*Δ cells. The recent work of Holthuis *et al.* (1998) provides another model for the function of Tlg2p. Interestingly, these authors demonstrate that, like four other t-SNAREs, Tlg2p binds the v-SNARE Vti1p in agreement with the data demonstrating the role of Vti1p in different vesicle transport pathways (Fischer von Mollard *et al*., 1997). Although Holthuis *et al.* (1998) report some observations very similar to ours, i.e., essentially normal CPY processing and invertase glycosylation, and a distinct endocytic defect in *tlg2*Δ cells, they propose that Tlg2p is located in the late Golgi compartment and is involved in a trafficking step from early endosomes back to the late Golgi. Our findings that *tlg2*Δ cells accumulate primary endocytic vesicles and are almost devoid of early endosomes appear difficult to fit with this hypothesis. However, in the absence of more extensive localization studies, we cannot entirely exclude that the endocytic delay we observe might be a secondary consequence of a defect in endosome back to late Golgi traffic.

It has been postulated that t-SNAREs act at every step of the secretory and endocytic pathways and that every cellular heterotypic fusion event is controlled by compartment-specific SNAREs (Hay and Scheller, 1997). Homotypic fusion between early endosomes was shown to require NSF protein (Rodriguez *et al*., 1994) and the Rab5 (Bucci *et al*., 1992). Here, we report that the t-SNARE Tlg2p is involved in an early step of endocytosis, i.e., entry into early endosomes or homotypic fusion of early endosomes. It was demonstrated recently that homotypic fusion can also be mediated by SNAREs; vacuolar fusion is mediated in yeast by a t-SNARE, Vam3p, and a v-SNARE, Nyv1p (Nichols *et al*., 1997). In mammals, the v-SNARE cellubrevin has been implicated in recycling endocytic receptors back to the plasma membrane (McMahon *et al*., 1993), but no t-SNARE has yet been implicated in the early steps of endocytosis.

ACKNOWLEDGMENTS

We are very grateful to C. Volland and D. Urban-Grimal for constructive discussions and critical reading of the manuscript and to I. Callebaut and P. Dehoux for their help with the sequence alignments. We thank A.-L. Haenni for critical reading of the manuscript and C. Jackson and T. Galli for fruitful advice. We thank C. Conesa, C. Holm, D. Wolf, T. Stevens, A. Franzusoff, Y. Wada, Y. Anraku, and J.R. Warner for generously providing antisera, plasmids, and strains. The work was supported by the European Community (EUROFAN within the framework of the Biotech program, to R.H.-T. and S.K.) and by grants from the Swiss National Science Foundation and the Swiss Federal Offfice for Education and Science (to H.R.), the Human Frontier Science Program (grant RG63/95 to S.K.), and the National Science Foundation (grant MCB-9604342) and the Pew Charitable Trusts (to B.S.G.).

REFERENCES

Aalto, M.K., Keränen, S., and Ronne, H. (1992). A family of proteins involved in intracellular transport. Cell *68*, 181–182.

Aalto, M.K., Ronne, H., and Keränen, S. (1993). Yeast syntaxins Sso1p and Sso2p belong to a family of related membrane proteins that function in vesicular transport. EMBO J. *12*, 4095–4104.

Abeliovich, H., Grote, E., Novick, P., and Ferro-Novick, S. (1998). Tlg2p, a yeast syntaxin homolog that resides on the Golgi and endocytic structures. J. Biol. Chem. *273*, 11719–11727.

Becherer, K.A., Rieder, S.E., Emr, S.D., and Jones, E.W. (1996). Novel syntaxin homologue, Pep12p, required for the sorting of lumenal hydrolases to the lysosome-like vacuole in yeast. Mol. Biol. Cell *7*, 579–594.

Benedetti, H., Raths, S., Crausaz, F., and Riezman, H. (1994). The *END3* gene encodes a protein that is required for the internalization step of endocytosis and for actin cytoskeleton organization in yeast. Mol. Biol. Cell *5*, 1023–1037.

Bennett, M.K., Calakos, N., and Scheller, R.H. (1992). Syntaxin: a synaptic protein implicated in docking of synaptic vesicles at presynaptic active zones. Science *257*, 255–258.

Bonneaud, N., Ozier-Kalogeropoulos, O., Li, G.Y., Labouesse, M., Minvielle-Sebastia, L., and Lacroute, F. (1991). A family of low and high copy replicative, integrative and single-stranded *S. cerevisiae/E. coli* shuttle vectors. Yeast *7*, 609–615.

Bucci, C., Parton, R.G., Mather, I.H., Stunnenberg, H., Simons, K., Hoflack, B., and Zerial, M. (1992). The small GTPase rab5 functions as a regulatory factor in the early endocytic pathway. Cell *70*, 715–728.

Burd, C.G., Peterson, M., Cowles, C.R., and Emr, S.D. (1997). A novel Sec18p/NSF-dependant complex required for Golgi-to-endosome transport in yeast. Mol. Biol. Cell *8*, 1089–1104.

Callebaut, I., Labesse, G., Durand, P., Poupon, A., Canard, L., Chomilier, J., Henrissat, B., and Mornon, J.-P. (1997). Deciphering protein sequence information through hydrophobic cluster analysis (HCA): current status and perspectives. Cell. Mol. Life Sci. *53*, 621–645.

Cowles, C.R., Emr, S.D., and Horazdovsky, B.F. (1994). Mutations in the *VPS45* gene, a *SEC1* homologue, result in vacuolar protein sorting defect and accumulation of membrane vesicles. J. Cell Sci. *107*, 3449–3459.

Cowles, C.R., Snyder, W.B., Burd, C.G., and Emr, S.D. (1997). Novel Golgi to vacuole delivery pathway in yeast: identification of a sorting determinant and required transport component. EMBO J. *16*, 2769–2782.

Davis, N.G., Horecka, J.L., and Sprague, J.G.F. (1993). Cis- and trans-acting functions required for endocytosis of the yeast pheromone receptors. J. Cell Biol. *122*, 53–65.

Dulic, V., Egerton, M., Elguindi, I., Raths, S., Singer, B., and Riezman, H. (1991). Yeast endocytosis assays. Methods Enzymol. *194*, 697–710.

Fischer von Mollard, G., Nothwehr, S.F., and Stevens, T.H. (1997). The yeast v-SNARE Vti1p mediates two vesicle transport pathways through interactions with the t-SNAREs Sed5p and Pep12p. J. Cell Biol. *137*, 1511–1524.

Franzusoff, A., Redding, K., Crosby, J., Fuller, R.S., and Schekman, R. (1991). Localization of components involved in protein transport and processing through the yeast Golgi apparatus. J. Cell Biol. *112*, 27–37.

Galan, J.M., Moreau, V., André, B., Volland, C., and Haguenauer-Tsapis, R. (1996). Ubiquitination mediated by the Npi1p/Rsp5p ubiquitin-protein ligase is required for endocytosis of the yeast uracil permease. J. Biol. Chem. *271*, 10946–10952.

Geli, M., and Riezman, H. (1998). Endocytic internalization in yeast and animal cells. J. Cell Sci. *111*, 1031–1037.

Gietz, D., St. Jean, A., Woods, R.A., and Schiestl, R.H. (1992). Improved method for high efficiency transformation of intact yeast cells. Nucleic Acids Res. *20*, 1425.

Goodson, H.V., Anderson, B.L., Warrick, H.M., Pon, L.A., and Spudich, J.A. (1996). Synthetic lethality screen identifies a novel yeast myosin I gene (*MYO5*): myosin I proteins are required for polarization of the actin cytoskeleton. J. Cell Biol. *133*, 1277–1291.

Götte, M., and Fischer von Mollard, G. (1998). A new beat for the SNARE drum. Trends Cell Biol. *8*, 215–218.

Gruenberg, J., and Maxfield, F. (1995). Membrane transport in the endocytic pathway. Curr. Opin. Cell Biol. *7*, 552–563.

Haas, A., Scheglmann, D., Lazar, T., Gallwitz, D., and Wickner, W. (1995). The GTPase Ypt7p of *Saccharomyces cerevisiae* is required on both partner vacuoles for the homotypic fusion step of vacuole inheritance. EMBO J. *14*, 5258–5270.

Hay, J.C., and Scheller, R.H. (1997). SNAREs and NSF in targeted membrane fusion. Curr. Opin. Cell Biol. *9*, 505–512.

Hicke, L., Zanolari, B., Pypaert, M., Rohrer, J., and Riezman, H. (1997). Transport through the yeast endocytic pathway occurs through morphologically distinct compartments and requires an active secretory pathway and Sec18p/*N*-ethylmaleimide-sensitive fusion protein. Mol. Biol. Cell *8*, 13–31.

Holthuis, J.C.M., Nichols, B.J., Dhruvakumar, S., and Pelham, H.R.B. (1998). Two syntaxin homologues in the TGN/endosomal system of yeast. EMBO J. *17*, 113–126.

Horazdovsky, B.F., Busch, G.R., and Emr, S.D. (1994). *VPS21* encodes a rab-like GTP binding protein that is required for the sorting of yeast vacuolar proteins. EMBO J. *13*, 1297–1309.

Jones, E.W., Webb, G.C., and Hiller, M.A. (1997). Biogenesis and function of the yeast vacuole. In: The Molecular and Cellular Biology of the Yeast Saccharomyces, vol. 3, Cell Cycle and Cell Biology, ed. J.R. Pringle, J.R. Broach, and E.W. Jones, Cold Spring Harbor, NY: Cold Spring Harbor Laboratory Press, 363–470.

Klionsky, D.J., Herman, P.H., and Emr, S.D. (1990). The fungal vacuole: composition, function and biogenesis. Microbiol. Rev. *54*, 266–292.

Kübler, E., Schimmoller, F., and Riezman, H. (1994). Calcium-independent calmodulin requirement for endocytosis in yeast. EMBO J. *13*, 5539–5546.

McMahon, H.T., Ushkaryov, Y.A., Edelmann, L., Link, E., Binz, T., Niemann, H., Jahn, R., and Südhof, T.C. (1993). Cellubrevin is a ubiquitous tetanus-toxin substrate homologous to a putative synaptic vesicle fusion protein. Nature *364*, 346–349.

Moreau, V., Galan, J.-M., Devilliers, G., Haguenauer-Tsapis, R., and Winsor, B. (1997). The yeast actin-related protein Arp2p is required for the internalization step of endocytosis. Mol. Biol. Cell *8*, 1361–1375.

Moreau, V., Madania, A., Martin, R.P., and Winsor, B. (1996). The *Saccharomyces cerevisiae* actin-related protein aArp2 is involved in the actin cytoskeleton. J. Cell Biol. *134*, 117–132.

Mumberg, D., Muller, R., and Funk, M. (1994). Regulatable promoters of *Saccharomyces cerevisiae*: comparison of transcritional activity and their use for heterologous expression. Nucleic Acids Res. *22*, 5767–5768.

Munn, A.L., and Riezman, H. (1994). Endocytosis is required for the growth of vacuolar H+ ATPase-defective yeast: identification of six new *END* genes. J. Cell Biol. *127*, 373–386.

Nichols, B.J., Ungermann, C., Pelham, H.R.B., Wickner, W.T., and Haas, A. (1997). Homotypic vacuolar fusion mediated by t- and v-SNAREs. Nature *387*, 199–202.

Niedenthal, R.K., Riles, L., Johnston, M., and Hegemann, J.H. (1996). Green fluorescent protein as a marker for gene expression and subcellular localization in budding yeast. Yeast *12*, 773–786.

Nilsson, I., Whitley, P., and von Heijne, G. (1994). The COOH-terminal ends of internal signal and signal-anchor sequences are positioned differently in the ER translocase. J. Cell Biol. *126*, 1127–1132.

Nothwehr, S.F., Conibear, E., and Stevens, T.H. (1995). Golgi and vacuolar membrane proteins reach the vacuole in *vps1* mutant yeast cells via the plasma membrane. J. Cell Biol. *129*, 35–46.

Novick, P., and Schekman, R. (1979). Secretion and cell-surface growth are blocked in a temperature-sensitive mutant of *Saccharomyces cerevisiae*. Proc. Natl. Acad. Sci. USA *76*, 1858–1862.

Novick, P., and Zerial, M. (1997). The diversity of Rab proteins in vesicles transport. Curr. Opin. Cell Biol. *9*, 496–504.

Ossig, R., Dascher, C., Trepte, H.-H., Schmitt, H.D., and Gallwitz, D. (1991). The yeast *SLY* gene products, suppressors of defects in the essential GTP-binding Ypt1 protein, may act in endoplasmic reticulum-to-Golgi transport. Mol. Cell. Biol. *11*, 2980–2993.

Pelham, H.R.B. (1998). Getting through the Golgi complex. Trends Cell Biol. *8*, 45–49.

Prescianotto-Baschong, C., and Riezman, H. (1998). Morphology of the yeast endocytic pathway. Mol. Biol. Cell *9*, 173–189.

Rayner, J.C., and Pelham, H.R.B. (1997). Transmembrane domain-dependant sorting of proteins to the ER and plasma membrane in yeast. EMBO J. *16*, 1832–1841.

Riezman, H. (1993). Yeast endocytosis. Trends Cell Biol. *3*, 273–277.

Riezman, H., Munn, A., Geli, M.I., and Hicke, L. (1996). Actin-, myosin- and ubiquitin-dependent endocytosis. Experientia *52*, 1033–1041.

Robinson, M.S., Watts, C., and Zerial, M. (1996). Membrane dynamics in endocytosis. Cell *84*, 13–21.

Rodriguez, L., Stirling, C.J., and Woodman, P.G. (1994). Multiple *N*-ethylmaleimide-sensitive components are required for endosomal vesicle fusion. Mol. Biol. Cell *5*, 773–783.

Rothstein, R. (1991). Targeting, disruption, replacement, and allele rescue: integrative DNA transformation in yeast. Methods Enzymol. *194*, 281–301.

Schimmöller, F., and Riezman, H. (1993). Involvement of Ypt7p, a small GTPase, in traffic from late endosome to the vacuole in yeast. J. Cell Sci. *106*, 823–830.

Sherman, F., Fink, G., and Hicks, J.B. (1983). Methods in Yeast Genetics: A Laboratory Manual, Cold Spring Harbor, NY: Cold Spring Harbor Laboratory Press.

Singer-Krüger, B., Frank, R., Crausaz, F., and Riezman, H. (1993). Partial purification and characterization of early and late endosomes from yeast. J. Biol. Chem. *268*, 14376–14386.

Singer-Krüger, B., Stenmark, H., and Zerial, M. (1995). Yeast Ypt51p and mammalian Rab5: counterparts with similar function in the early endocytic pathway. J. Cell Sci. *108*, 3509–3521.

Söllner, T., Whiteheart, S.W., Brunner, M., Erdjument-Bromage, H., Geromanos, S., Tempst, P., and Rothman, J.E. (1993). SNAP receptors implicated in vesicle targeting and fusion. Nature *362*, 318–324.

van Tuinen, E., and Riezman, H. (1987). Immunolocalization of glyceraldehyde-3-phosphate dehydrogenase, hexokinase, and carboxypeptidase Y in yeast cells at the ultrastructural level. J. Histochem. Cytochem. *35*, 327–333.

Vernet, T., Dignard, D., and Thomas, D.Y. (1987).A family of yeast expression vectors containing the phage f1 intergenic region. Gene *52*, 225–233.

Vida, T.A., and Emr, S. (1995). A new vital stain for visualizing vacuolar membrane dynamics and endocytosis in yeast. J. Cell Biol. *128*, 779–792.

Volland, C., Urban-Grimal, D., Géraud, G., and Haguenauer-Tsapis, R. (1994). Endocytosis and degradation of the yeast uracil permease under adverse conditions. J. Biol. Chem. *269*, 9833–9841.

Wach, A. (1996). PCR-synthesis of marker cassettes with long flanking homology regions for gene disruptions in *S. cerevisiae*. Yeast *12*, 259–265.

Wach, A., Brachat, A., Pöhlmann, R., and Phippsen, P. (1994). New heterologous modules for classical or PCR-based gene disruptions in *Saccharomyces cerevisiae*. Yeast *10*, 1793–1808.

Wada, Y., Kitamoto, K., Kanbe, T., Tanaka, K., and Anraku, Y. (1990). The *SLP1* gene of *Saccharomyces cerevisiae* is essential for vacuolar morphogenesis and function. Mol. Cell. Biol. *10*, 2214–2223.

Wada, Y., Nakamura, N., Ohsumi, Y., and Hirata, A. (1997). Vam3p, a new member of syntaxin related protein, is required for vacuolar assembly in the yeast *Saccharomyces cerevisiae*. J. Cell Sci. *110*, 1299–1306.

Weimbs, T., Hui Low, S., Chapin, S.J., Mostov, K.E., Bucher, P., and Hofmann, K. (1997). A conserved domain is present in different families of vesicular fusion proteins: a new superfamily. Proc. Natl. Acad. Sci. USA *94*, 3046–3051.

Wichman, H., Hengst, L., and Gallwitz, D. (1992). Endocytosis in yeast: evidence for the involvement of a small GTP-binding protein (Ypt7p). Cell *71*, 1131–1142.

Wilcox, C.A., Redding, K., Wright, R., and Fuller, R.S. (1992). Mutation of a tyrosine localization signal in the cytosolic tail of yeast Kex2 protease disrupts Golgi retention and results in default transport to the vacuole. Mol. Biol. Cell *3*, 1353–1371.

Winston, F., Dollard, C., and Ricupero-Hovasse, S.L. (1995). Construction of a set of convenient *Saccharomyces cerevisiae* strains that are isogenic to S288C. Yeast *11*, 53–55.